

11-2011

Thermal comparison between ceiling diffusers and fabric ductwork diffusers for green buildings

Anthony Fontanini

Iowa State University


Michael Olsen

Iowa State University, mgolsen@iastate.edu

Baskar Ganapathysubramanian

Iowa State University, baskarg@iastate.edu

Follow this and additional works at: http://lib.dr.iastate.edu/me_pubs

 Part of the [Energy Systems Commons](#), [Heat Transfer, Combustion Commons](#), and the [Power and Energy Commons](#)

The complete bibliographic information for this item can be found at http://lib.dr.iastate.edu/me_pubs/221. For information on how to cite this item, please visit <http://lib.dr.iastate.edu/howtocite.html>.

This Article is brought to you for free and open access by the Mechanical Engineering at Iowa State University Digital Repository. It has been accepted for inclusion in Mechanical Engineering Publications by an authorized administrator of Iowa State University Digital Repository. For more information, please contact digirep@iastate.edu.

Thermal comparison between ceiling diffusers and fabric ductwork diffusers for green buildings

Anthony Fontanini, Michael G. Olsen,
and Baskar Ganapathysubramanian¹

Department of Mechanical Engineering, 2100 Black Engineering, Iowa State University, Ames, IA 50010, USA

Abstract

Continuously increasing energy standards have driven the need for increasing the efficiency of buildings. Most enhancements to building efficiency have been a result of changes to the heating/cooling systems, improvements in construction materials, or building design code improvements. These approaches neglect the way in which air is dispersed into individual rooms or in a building - i.e., the ducting system. This opens up the possibility of significant energy savings by making ductwork systems lighter and better insulating while ensuring cost effectiveness.

The current study explores this idea by comparing the performance of conventional ductwork with recent advancements in fabric-based ductwork. We focus on the transient behavior of an on/off control system, as well as the steady state behavior of the two ductwork systems. Transient, fully three dimensional validated computational (CFD) simulations are performed to determine flow patterns and thermal evolution in rooms containing either conventional or fabric ductwork. This analysis is used to construct metrics on efficiency. A number of different flow rates are examined to determine the performance over a range of operating conditions. Transient finite volume simulations consisted of over 13 million degrees of freedom for over 10,000 time steps. The simulations utilized HPC (High Performance Computing) for the large scale analysis.

The results conclusively show that fabric ducting systems are superior to the conventional systems in terms of efficiency. Observations from the data show that fabric ducting systems heat the room faster, more uniformly, and more efficiently. The increase in performance demonstrates the potential benefits of moving away from conventional systems to fabric systems for the construction of green buildings: particularly in conjunction with adaptive control systems.

Key words: Green buildings; ductwork; thermal management; computational fluid dynamics; high performance computing; fabric ducting;

1 Introduction

The design of efficient building systems is necessary for meeting increasing energy standards. This trend pushes designers to create green buildings. Numerous strategies are available for increasing the energy efficiency of buildings: energy collection systems such as solar power cells can decrease the energy load in the building [12], solar water heating systems can preheat water to cover a large fraction of the heating demand [31], and materials such as aerogels and phase change materials (PCMs) can help increase the thermal resistance of building envelope components [14,15]. Control and supervision of heating ventilation and air conditioning (HVAC) systems can optimize the task of efficiently moving the energy through the building [4,29]. In addition, architectural design can create spaces that are both aesthetically pleasing and energy efficient [2]. Each of these approaches have aided in decreasing the amount of energy needed to operate green buildings.

Most energy saving systems used in green buildings have neglected a significant component of HVAC systems, the ductwork system. Conventional ductwork systems comprised of sheet metal ductwork and diffusers have a number of features that can adversely affect their performance. The conduction of heat through the sheet metal leads to a loss in energy as the air is dispersed in the building. Coatings can be added to the ductwork to make them less conductive, but the coatings lead to additional costs in the system. Moreover, the ductwork is heavy, and needs extra parts for support. Most importantly, the non-homogeneous nature of the airflow generated by diffusers leads to non-uniformities in heating/cooling causing discomfort. Finally, placement of conventional diffusers becomes a significant design decision in the effort to minimize local hot/cold spots and unpleasant drafts within the space.

Recent advances in ductwork technology has shown promise towards enhancing building efficiency. Figure 1(b) shows a ventilation system where an *insulating fabric* ductwork has been used to transport air to desired locations within the building, thus limiting energy loss to non-desirable areas and eliminating the need for a coating to make the ductwork less conductive. Furthermore, the fabric weighs much less than conventional sheet metal ductwork, removing the need for extra parts for support and further reducing costs. Along the length of the ducting, a series of strategically placed holes disperses the air uniformly throughout the desired space².

¹ Corresponding author: Ganapathysubramanian, Fax: 515 294-3261, Email: baskarg@iastate.edu, URL: <http://www3.me.iastate.edu/bglab/>

² The number and size of holes placed in each desired room affects the power and static pressure required by the fan to a small extent. However, in multi-room buildings the fan power used will depend more on the major and minor losses of the ducting system that reaches the individual space rather than the specific air

In addition to the general benefits of fabric ducting, fabric ducting aims toward producing uniform and low-draft air supply in the desired space. Recent technology trends such as stratum ventilation (SV) and personal ventilation (PV) strive to create such a personalized local climate for medium and small room sizes. Personal ventilation provides a tailored environment for each individual, for each individual has their own sensitivity to air movement or air quality [19]. In personal ventilation, an individual trying to increase the air quality can be strongly affected by a turbulent jet provided by the PV system [23]. Similarly, stratum ventilation creates a layer of fresh air within the breathing zone of the occupants [28]. The attention to the breathing zone in SV systems provides better indoor air quality, but can still suffer from the effects of uncomfortable drafts from turbulent jets. Fabric ducting can be naturally incorporated into the PV and SV systems to provide the necessary uniform quality airflow required by the occupants without the negative effects of turbulent high-draft jets.

The positive aspects of fabric systems directly improve upon the drawbacks of conventional sheet metal diffuser systems. Currently, limited data is available to evaluate either type of system with respect to air coverage and thermal performance. The present work consists of numerical simulations that directly compare conventional ceiling diffuser systems and fabric systems to quantify the increase in performance of the fabric systems in both the initial transient period and steady state operating conditions. Three dimensional, full-scale, time-varying realistic simulations have been performed to allow for direct comparisons. The simulations show the time evolution of the temperature field within the rooms. The simulations provide qualitative observations that can aid in future design decisions, in addition to quantitative data that provide a direct measure of the performance and comfort level of the room through time.

2 Problem definition

The problem the present work seeks to address is to compare fabric-based ductwork to conventional sheet-metal ductwork quantitatively based on measures of efficiency. The physical space being studied represents an individual office space or a bed room. The simulations performed represent a room that has been unattended during the night, which is typical for an office space. At a given time in the morning the heating system is turned on in anticipation for another working day. Metrics for efficiency (and comfort) include mean and standard deviation of both air speed and temperature, the amount of power absorbed by the room, the Air Distribution Performance Index (ADPI), and

distribution mechanism within an individual room.

the energy used and time taken to heat the room to an average temperature of 290.94 Kelvin.

The simulations are performed in a 2.43 m \times 2.43 m \times 2.43 m [8 ft \times 8 ft \times 8 ft] domain, which is a typical configuration in office spaces. The air outlet is placed on the ceiling for a *worst case scenario* in which the return air outlet is near the inlet. The outlet was offset 0.61 m [2 ft] in the x-direction, and has dimensions of 0.30 m \times 0.30 m [1 ft \times 1 ft]. The inlet for the diffuser is placed on the ceiling in the center of the domain (Fig. 2 (a),(b)), and the inlet for the fabric ductwork is placed on the side wall (Fig. 2 (c),(d)).

For the fabric ductwork system, the air flow travels through the ducting tube until the air reaches the edge of the domain in the z-direction where another wall is encountered. The air is forced through 7 pairs of 2.54 cm [1 in] diameter holes spaced 0.30 m [1 ft] apart. The tube's center is 2.13 m [7 ft] above the floor. In the case of the conventional system, the diffuser inlet is 15.24 cm [6 in] in diameter. The bottom of the diffuser is 55.88 cm [22 in] long in both the x and z directions, and protrudes downward 15.24 cm [6 in] into the domain.

The flow patterns and thermal evolution in each room are simulated for different flow rates (shown in Table 3) to quantify performance and efficiency. The flow rates correspond to multiples of ASHRAE's minimum required flow rate for an office space. The room and the walls are heated from an initial temperature of 288.67 Kelvin [60 F] by an inlet air supply at 299.56 Kelvin [80 F]. The walls are maintained at the initial temperature of the room.

3 Simulation Methodology

3.1 Basic Equations

The basic equations describing the thermo-fluid phenomena are the Navier-Stokes equations, conservation of mass, and conservation of energy. Variables used in subsequent developments are defined in Table 1. Note however that these basic equations have to be augmented with aspects of buoyancy, compressibility, and turbulence, which are discussed in the subsequent sections.

3.2 Compressibility and Buoyancy

Air flow can be considered incompressible if the velocities within the room are sufficiently small. The Mach number provides a gauge on the significance of compressibility effects, and if the Mach number is less than 0.3 the flow can

be considered incompressible [6]. The Mach number was calculated using the equation [6], $Ma = \frac{\sqrt{u_i u_i}}{c}$. Posteriori processing revealed that the incompressible assumption is valid.

Typically, air flows in buildings are driven by both inertial and buoyancy forces. Buoyancy forces have a large effect on fluid flow within buildings. The buoyancy forces can be approximated by the Boussinesq approximation if the density changes linearly with temperature through the operating temperature range. The Boussinesq approximation is added as a force term to the y-component of the conservation of linear momentum equation as

$$f_y = -\rho g_y \beta (T_\infty - T) \quad (1)$$

We ensured that the Boussinesq assumption is strictly valid in the temperature range [6] used in all the simulations.

3.3 Turbulence Modeling

The inlet Reynolds numbers for both systems for all flow rates are in the turbulent range. An appropriate choice of the turbulence model is key to ensuring accurate solutions. The k - ϵ model is a simple, computationally inexpensive turbulence model, and has been shown to have the largest range of applicability. The k - ϵ model is a Reynolds Averaged Navier-Stokes (RANS) model. The model assumes that the flow is composed of a mean flow component and a fluctuating component ($u = \bar{u} + \tilde{u}$)[22]. The turbulent Reynolds stresses and the turbulent heat fluxes are resolved by the eddy-viscosity concept [3]. The governing equations are:

Conservation of Linear Momentum

$$\rho \left(\frac{\partial \bar{u}_m}{\partial t} + \bar{u}_i \frac{\partial \bar{u}_m}{\partial x_i} \right) = -\frac{\partial \bar{p}}{\partial x_m} + \frac{\partial}{\partial x_m} \left[(\mu + \mu_T) \left(\frac{\partial \bar{u}_j}{\partial x_i} + \frac{\partial \bar{u}_i}{\partial x_j} \right) \right] - \rho g_y \beta (\bar{T}_\infty - \bar{T}) \quad (2)$$

Conservation of Mass

$$\frac{\partial \rho}{\partial t} + \frac{\partial}{\partial x_i} (\rho \bar{u}_i) = 0 \quad (3)$$

Conservation of Energy

$$\frac{\partial}{\partial t} (\rho c_p \bar{T}) + \frac{\partial}{\partial x_i} (\rho c_p \bar{u}_i \bar{T}) = \frac{\partial}{\partial x_i} \left[\left(\alpha + \frac{c_p \mu_T}{\sigma_t} \right) \frac{\partial \bar{T}}{\partial x_i} \right] \quad (4)$$

The turbulent viscosity term is dependent on two parameters k and ε , the turbulent kinetic energy and turbulent dissipation, respectively [22],

$$\varepsilon = \frac{C_\mu \rho k^2}{\mu_T} \quad \text{and} \quad k = \frac{1}{2} (\bar{u}_i \bar{u}_i) \quad (5)$$

where C_μ is an empirical constant. The addition of the two parameters requires two more equations to solve the system of equations. The two additional equations are the transport equations for k and ε , where σ_k , σ_ε , C_1 , and C_2 are all empirical constants.

$$\begin{aligned} \frac{\partial}{\partial t} (\rho k) + \frac{\partial}{\partial x_i} (\rho k u_i) &= \frac{\partial}{\partial x_i} \left(\frac{\mu_T}{\sigma_k} + \frac{\partial k}{\partial x_i} \right) \\ &+ \mu_T \left(\frac{\partial u_i}{\partial x_j} + \frac{\partial u_j}{\partial x_i} \right) \frac{\partial u_i}{\partial x_j} - \rho \varepsilon - g \beta \frac{\mu_T}{\sigma_t} \frac{\partial T}{\partial y} \end{aligned} \quad (6)$$

$$\begin{aligned} \frac{\partial}{\partial t} (\rho \varepsilon) + \frac{\partial}{\partial x_i} (\rho \varepsilon u_i) &= \frac{\partial}{\partial x_i} \left(\frac{\mu_T}{\sigma_\varepsilon} + \frac{\partial \varepsilon}{\partial x_i} \right) \\ &+ C_1 \frac{\varepsilon}{k} \mu_T \left(\frac{\partial u_i}{\partial x_j} + \frac{\partial u_j}{\partial x_i} \right) \frac{\partial u_i}{\partial x_j} - C_2 \rho \frac{\varepsilon^2}{k} \\ &- C_1 g \frac{\varepsilon}{k} \beta \frac{\mu_T}{\sigma_t} \frac{\partial T}{\partial y} \end{aligned} \quad (7)$$

The system of equations can then be solved simultaneously for pressure, temperature, turbulent kinetic energy, turbulent dissipation, and velocity in the x, y, and z directions.

3.4 Boundary Conditions

All of the walls (i.e. the four side walls, the ceiling, and the floor), the diffuser, and the tube had no slip conditions applied for the velocity. All the walls were maintained at 288.67 Kelvin. The outlet was a 0 gauge pressure outlet. Conduction through the diffuser and tube was neglected in these simulations. To test the performance of the different systems at different flow rates, the inlet volumetric flow rate was varied according to Table 3. The smallest flow rate was chosen based on the minimum flow rate for a bedroom/living room/office

space for two people occupying a space of this size from ASHRAE design standards [9]. The flow rate was increased to approximately 2, 5, 10, and 21 times the minimum flow rate. The inlet flow temperature was held constant at 299.56 Kelvin.

3.5 Domain Discretization

The numerical approach to solving these equations begins with a finite volume discretization of each domain. The domains for both the diffuser and the fabric ducting system have relatively complex geometry. This geometry leads to large velocity gradients in some parts of the domain and small velocity gradients in other parts of the domain. Therefore, to save on computational time and computer memory, an adaptive meshing technique was used to place a higher density of elements near the diffuser, the fabric tube, and the outlets, while a smaller element density is used near the center and edges of the domain.

3.6 Solution Procedure

The commercial CFD software Fluent [1] was used to solve the coupled set of governing equations. The momentum, turbulent kinetic energy, turbulent dissipation rate, and energy equations were solved using second order spatial upwind methods. The transient formulation used a first order implicit algorithm. The time step for each simulation was chosen by satisfying the CFL (Courant-Friedrichs-Lewy) number (using the cubed root of the smallest element volume for the smallest distance). The calculation of the diffusion terms, the velocity derivatives, and the construction of scalar values at the cell faces, was done by a Least Squares Cell-Based method. The properties of air were taken at an average temperature between the inlet and the outlet.

3.7 High Performance Computing

The domains were discretized into roughly 0.5 million elements, 1 million elements, and 2 million elements to check for numerical convergence (see Section 3.8). All results shown in this paper are from the finest resolution simulations. For each element, residuals for the x velocity, y velocity, z velocity, continuity, energy, k and ε were computed. The number of degrees of freedom (DOF) in the simulations ranged from 3.5 - 14 million for each time step over 10,000 time steps. High Performance computing (HPC) was used to solve the large number of DOF. Computational time on a HPC cluster ABE through the National Center for Supercomputing Applications (NCSA) [13] was utilized for

these simulations. The cluster enabled the simulations to be run at a much more efficient rate, and allowed more than one simulation to be run at one time.

3.8 Verification and Validation

We perform verification and validation to ensure the accuracy of our simulation in four steps. First, the CFD model is checked with experimental results to ensure that the model reproduces the turbulent jet characteristics near the diffuser and fabric ductwork inlets. Next, the wall shear stresses produced are checked to ensure validity of not using any special wall functions. Subsequently, we ensure that the airflow and turbulent statistics far from the inlet jet region are accurately captured using this CFD model in a full scale building simulation. Finally, a comprehensive convergence analysis was performed for three different grid/mesh densities and resolutions that ensures spatial accuracy of the results. We detail each of these steps below.

- (1) The air flow near the diffuser and fabric ductwork inlets can be characterized as turbulent jets³. Proper resolution of this jet region is essential, for inaccuracies are propagated downstream to the rest of the domain. We have extensively studied and evaluated RANS models of turbulence for the near-wake, intermediate-wake, and far-wake regions of a turbulent jet. The CFD model validation in the three different wake regions have been done in our previous work, in particular the experiments and simulations conducted by Liu et al. [18] and Feng et al. [10] which investigate the performance of the $k - \varepsilon$ model against PIV and PLIF experiments at different downstream locations of a turbulent jet. The results from Liu et al. [18], establish that the $k - \varepsilon$ model replicate with excellent agreement the streamwise velocity, turbulent kinetic energy, and turbulent dissipation of the turbulent jet. The results from Feng et al. [10] ensure that as the turbulent jet propagates downstream, the $k - \varepsilon$ model maintains accuracy with the streamwise velocity.
- (2) The $k - \varepsilon$ model accurately approximates the velocity and heat transfer within the boundary layer near a solid boundary when the wall shear stresses produced by the turbulent flow are low when compared with the maximum shear stress in the domain [3]. In the current simulations, the maximum shear stress produced at the wall was 0.038 Pa for the diffuser system and 0.074 Pa for the fabric system. The maximum shear stress at the jet exits were 0.33 Pa for the diffuser system and 0.91 Pa for the fabric

³ The scale of the jets for each case occupied less than 1.1% by volume of the domain based on the velocity decreasing by 90% from the maximum. However, they bring in most of the turbulent kinetic energy into the domain.

system. Since the shear stress was significantly small near the walls, the $k - \varepsilon$ model performs well and no special wall functions are needed.

- (3) The use of RANS models (specifically the $k - \varepsilon$ model) to simulate non-isothermal and isothermal airflow within full scale buildings have been rigorously validated using PIV based experiments [26,27] performed recently. The experimental and computational studies from H. Sun et al.[27] show that over 70% of the velocity field (far from the inlet jet region) is accurately represented by the $k - \varepsilon$ model when compared to the PIV results. We utilize the same implementation to ensure accurate characterization of the flow field far from the inlet jet region.
- (4) Three sets of increasingly refined meshes were generated to perform convergence tests. Table 2 shows the number of degrees of freedom in each domain for the convergence test. The conventional system and the fabric system were simulated on three increasingly resolved discretized domains, consisting of approximately 0.5 million elements, 1 million elements, and 2 million elements. The convergence analysis was performed for the largest flow rate. Achieving convergence at the maximum flow rate also ensured that the discretization for lower flow rates were spatially converged. The error is reported in terms of the L_2 norm error

$$L_2(x) = \frac{\sqrt{\sum_{i=1}^n |x_i - x_i^{(ideal)}|^2}}{\sqrt{\sum_{i=1}^n |x_i^{(ideal)}|^2}} \quad (8)$$

where x is the quantity of interest which are: the mean and standard deviation of the temperature field, the mean and standard deviation of the air speed in the room, and the amount of power being absorbed by the room. The L_2 error was calculated using the solution on the finest resolution grid (2 million element discretization) as the resolved (ideal) solution. A small value of the L_2 norm error indicates that the solutions do not change with improving resolution thus representing convergence. Table 4 displays the L_2 error in the results.

3.9 Metrics of Comparison: Comfort and Efficiency

To help quantitatively compare the performance of the two systems, we utilized a set of metrics that represent notions of efficiency. One set of metrics used was the time evolution of mean and standard deviation for the temperature and velocity fields. The mean and standard deviation of the temperature field gave information on how quickly and homogeneously the room was heating. The air speed mean and standard deviation gave information on the extent of the "draftiness" of the room. A weighted volume average was used for the

mean and standard deviation (due to the non-uniform discretization of the domain).

$$\phi_T = \sum_{i=1}^n T_i \frac{V_i}{V_T} \quad \text{and} \quad \sigma_T = \sqrt{\sum_{i=1}^n V_i (T_i - \phi_T)^2} \quad (9)$$

where ϕ_T is the mean of the temperature field, V_i is the volume of cell i , V_T is the total volume ($V_T = \sum_{i=1}^n V_i$), n is the number of cells, and σ_T is the standard deviation of the temperature field. We similarly define the mean and standard deviation of the velocity field.

$$\phi_u = \sum_{i=1}^n u_i \frac{V_i}{V_T} \quad \text{and} \quad \sigma_u = \sqrt{\sum_{i=1}^n V_i (u_i - \phi_u)^2} \quad (10)$$

where ϕ_u is the mean of the velocity field, and σ_u is the standard deviation of the velocity field.

The power that is absorbed by the room is expressed in terms of the rate of change of the mean temperature of the room.

$$\dot{E}_{absorbed} = \rho V_T c_p \frac{d\phi_T}{dt} \quad (11)$$

The total energy absorbed is computed by integrating the area under this (power absorbed vs time) curve.

In order to gain a quantitative sense of the comfort of the room a common metric is the Air Distribution Performance Index (ADPI). The ADPI is the percentage of the occupied zone that satisfies the requirements of the effective draft temperature and local air velocity. The effective draft temperature is a balance between thermal and convective comfort.

$$\theta = (t_x - \phi_T) - 0.07(V_x - 30) \quad (12)$$

where θ is the effective draft temperature, t_x is the local air temperature (F), and V_x is the local airstream velocity (fpm). An individual location within a room is deemed comfortable if the effective draft temperature is between -3 and +2 degrees Fahrenheit and the local air velocity is less than 70 feet per minute [21]. Therefore, in a room the higher the ADPI the more comfortable the room.

4 Results and Discussion

The simulations for both domains (diffuser and fabric ductwork) were performed for a cube shaped room with a volume of 14.35 m^3 . The simulated flow rates were 21, 10, 5, 2, and 1 times the ASHRAE recommended minimum flow rate for a small room with two people occupying the space [9]. The performance of the diffuser and fabric systems were first directly compared at the *largest flow rate*. The other flow rates (10, 5, 2, and 1 times the minimum flow rate) were compared against the largest flow rate for each system. The comparison of the systems included an evaluation of the performance in terms of efficiency metrics. The metrics used include (a) the mean and standard deviation of the temperature field within the room, (b) the mean and standard deviation of the air speed within the room, (c) the time taken to increase the mean temperature of the room to a more comfortable level, (d) the amount of power being absorbed by the room over time, and (e) the power necessary and the time required to raise the temperature of the room to a more comfortable level.

4.1 Flow Rate Analysis: Throw Diffuser

The diffuser system was simulated for five different flow rates as shown in Table 3. Each simulation computed the thermal and flow field evolution in the domain for a real-time duration of $t = 50$ seconds. Figure 3 shows iso-contours of temperature for the diffuser system at $t = 50$ seconds for the minimum flow rate recommended by ASHRAE, and also at 21 times the minimum flow rate. From Fig. 3, it is apparent that the minimum flow rate does not produce enough flow to actually heat the room. The warm air that is brought into the room stays along the ceiling never penetrating to the lower regions of the room. For the largest flow rate tested, shown in Fig. 3(d), the diffuser system was able to force the warm air far enough into the room so the entire room could be heated.

As the flow rate was increased, all but one of the metrics (mean room temperature, mean air speed, STD of air speed, and power absorbed by the room) also increased, which can be seen in Figs. 4(a), 5, and 6. The increase in all the metrics aids in the increase of the power absorbed by the room, as seen in Fig. 6⁴. The trend of increasing metrics occurred for all the metrics except for the temperature standard deviation of the room, as can be seen in Fig. 4(b). When the results of Fig. 4(b) are coupled with Fig. 3 the conclusion can be drawn that the mode shift seen in the temperature standard deviation could

⁴ For the flow rates chosen, higher flow rates resulted in an increase in the efficiency

be attributed to the increase in heating and mixing within the room. The increase in mixing causes the temperature standard deviation to decrease, thus resulting in a more homogeneous temperature distribution within the room. The continuous stream of fresh air ensures that there is reasonable recirculation of stale air. The focus of the simulations are in the transients when the room is first heated. At this time the rooms are assumed to be unoccupied. Hence, the IAQ (Indoor Air Quality) is not affected since the quality of the air coming into the room is assumed to be the same as the air in the room at the initial condition. The decrease in temperature standard deviation is a desired outcome and suggests a more homogeneously heated room.

The effects of the increase in mixing can also be seen in Fig. 5(a), where the mean air speed of the room increases dramatically between 10 times the minimum flow rate and 21 times the minimum flow rate. The large increase in velocity in Fig. 5(a), the temperature standard deviation mode shift in Fig. 4(b), and the temperature contour plots of Fig. 3 are indications the system is changing from a buoyancy driven flow to an inertial driven flow, thus enhancing mixing/heating.

4.2 Flow Rate Analysis: Fabric System

The fabric system was also simulated for the same volumetric flow rates as the diffuser system. Figure 7 shows the domain after $t = 50$ seconds for the ASHRAE's minimum and 5 times recommended flow rate. As in the diffuser case, the ASHRAE minimum flow rate and 2 times the minimum flow rate was not sufficient enough to heat the room. However, contours extend down into the room farther than the diffuser system. The warmer air did reach the floor in the simulations of 5, 10, and 21 times the minimum recommended flow rate.

For most of the metrics of efficiency, the fabric system displays similar behavior as the diffuser system in that the metrics increase as the flow rate increases. The mean temperature of the room increases as the flow rate increases as seen in Fig. 8(a). As expected, the mean air speed and the air speed standard deviation increases with flow rate as seen in Figs. 9(a) and 9(b). These trends represent increase of mixing and associated improvement in thermal performance. This results in more efficient heating as displayed by the net amount of energy absorbed by the room shown in Fig. 6.

Similar to the diffuser case, the exception to the increasing trend is the temperature standard deviation within the room which can be seen in Fig. 8(b). However, the mode shift occurs earlier for the fabric system than the diffuser system. The mode shift (from a predominantly buoyant flow to an inertial

flow) occurs between 2 times the ASHRAE minimum flow rate, and 5 times the ASHRAE minimum flow rate. The increase in mixing efficiency reduces the temperature standard deviation.

4.3 Analyzing the mode-shift: buoyant versus inertial flows

From the individual comparison of the two systems, both the fabric and diffuser systems exhibited a mode shift in the heating mechanism from a buoyancy driven system to a more inertial driven system as seen in the contour plots of Figs. 3 and 7. This mode-shift is mimicked by temperature standard deviation, which can be seen in Figs. 4(b) and 8(b). The Richardson number, the ratio of buoyancy forces to inertial forces, was calculated to characterize and confirm this change. The Richardson number is defined by $Ri = g\beta L_c (T_{in} - T_\mu) / V_\mu^2$, where Ri is the Richardson number, g is acceleration due to gravity, β is the coefficient of thermal expansion, L_c is the characteristic length of the room (taken to be the height of the room), T_{in} is the temperature of the air entering the room, T_μ is the mean temperature of the room at $t = 50$ seconds, and V_μ is the mean airflow of the room at $t = 50$ seconds.

The Richardson number for the diffuser system is approximately one order of magnitude higher than the fabric system as seen in Fig. 10. This means that overcoming the buoyant forces in the diffuser system is much harder than the fabric system. This results in the diffuser system needing a higher flow rate to overcome the critical Richardson number to cause the mode shift in the temperature standard deviation (due to an increase in mixing). Also note that this earlier mode-shift can also be attributed to the higher momentum of the fluid exiting the fabric ducting, making it easier for the fluid to overcome the buoyant forces thus enhancing mixing. The critical Richardson number occurs between the 10 and 21 times the ASHRAE minimum flow rate for the diffuser system, and 2 and 5 times the ASHRAE minimum flow rate for the fabric system.⁵

4.4 Comparing the Diffuser System with the Fabric System: Transient and Steady State Behavior

Iso-contours of the temperature for the diffuser and fabric system at the highest flow rate are shown in Figs. 11 and 12. Figures 11 and 12 indicate the

⁵ Since the mode shift only occurred in the largest flow rate, and since the highest flow rate is the only flow rate in which both rooms were fully heated, subsequent direct comparison between the two system was only done for the largest flow rate.

presence of fewer temperature contours in the fabric system room than the diffuser system. This shows that the temperature distribution of the diffuser system had warm and cold spots within the room. In contrast, the fabric system presented a more uniform temperature distribution after 50 seconds. Lower air velocities created by the diffuser were significantly affected by the outlet as the air flow entered the room. In the diffuser system, the airflow was drawn towards the outlet, which caused the temperature distribution in the room to be unsymmetrical. The smaller holes in the fabric system help force the airflow down into the room due to greater fluid momentum and the outlet subsequently had little effect on the airflow.

The diffuser and fabric systems were compared directly using the quantitative metrics used in the individual analysis of both systems. The temperature field was used to investigate and compare important measures for efficiency (and in some sense, comfort), which indicated the overall mean temperature of the room, volumes of high temperature gradients, and warm/cold spots within the space. Figure 13 shows that the mean temperature of the fabric ducting system increased more rapidly than the throw diffuser system. The faster increase in temperature resulted in the fabric system requiring 37.75 seconds and 67.61 kilowatts to increase the temperature of the room to 290.94 Kelvin as compared to 50.00 seconds and 89.54 kilowatts for the throw diffuser system. Figure 13 shows that the standard deviation of the temperature distribution was smaller in the fabric ducting system than the throw diffuser system. *The increase in the standard deviation of the diffuser system was due to the warm and cold spots near the floor and ceiling as seen in Fig. 12.* The fabric system thermally performed better than the throw diffuser system in the context of reducing warm and cold spots for a given flow rate.

The air speed within the room provides a specific metric on drafts within the room, indicating the overall breeziness of the room. Figure 14 shows that for the particular flow rate chosen, the diffuser had a smaller mean air speed within the room. The smaller holes of the fabric ductwork increase the air speed within the room. Figure 14 shows that the large air speeds within the fabric ductwork room were localized since the standard deviation was much larger than the diffuser system. The larger air speeds within the fabric ductwork room do allow the fresh warm airflow to penetrate farther into the room. The better penetration allows for better air quality in the breathing zones of the occupants. The diffuser system showed lower and more uniform air speeds than the fabric system for the chosen flow rate. This is the only metric where the diffuser system out-performs the fabric system.

The power being absorbed by the room illustrates how the energy input into the room was being utilized. Figure 15 shows that the fabric system absorbs more power than the diffuser system. A larger percentage of the power brought into the room by the fabric system was being used to heat the room. The

smaller fluid momentum for the diffuser system contributed to less power being utilized by the room. For the diffuser system, a significant fraction of air brought into the room stayed along the ceiling, causing large amounts of energy to escape out the outlet. The fabric system needed 21.93 less kilowatts and 12.25 less seconds to heat the room to 290.94 Kelvin (the final mean temperature of the diffuser room), which correlated to an *energy savings of 24.5% over the ceiling diffuser system in the transient period*.

A steady state analysis was done for both the diffuser and fabric systems. The steady state condition was determined to be after the initial transience of the mean velocity and the standard deviation of velocity within the room. In the steady state condition each system was evaluated in terms of comfort. In terms of comfort the ADPI for each flow rate was evaluated.

The comfort of the room is expressed in ADPI, a large value of ADPI represents the percentage of the occupied zone that is comfortable for a high percentage of occupants. The diffuser system, at low flow rates the room has a low ADPI, and at higher flow rates a high ADPI as seen in Fig. 16. The low ADPI for the diffuser system under lower flow rates is due to the low velocities and the large thermal gradients within the room. As the flow rate increased the ADPI increased for the diffuser system. The increase is attributed to the airflow starting to circulate in the occupied zone, and the high thermal and velocity gradients located near the walls which is outside the occupied zone.

The fabric system displayed to opposite behavior than the diffuser system. At low flow rates the ADPI value is high, and at higher flow rates the ADPI is small as seen in Fig. 16. The high ADPI values at low flow rates are due to the penetration of the air into the domain from the small holes of the fabric system. As the flow rate increases the ADPI drops, because the local air velocity grows farther away from 30 feet per minute.

Both the diffuser system and the fabric system display a sudden jump in ADPI between characteristic flow rates. The jump occurs between $0.037 \text{ m}^3/\text{s}$ and $0.065 \text{ m}^3/\text{s}$ for the fabric system and $0.065 \text{ m}^3/\text{s}$ and $0.140 \text{ m}^3/\text{s}$ for the diffuser system. The jump occurs at the same point at which the mode shift occurs in the transient temperature standard deviation. The jump for each system can be attributed to the point at which the air can penetrate to the floor of the room. From Fig. 16 the fabric system is more comfortable in the lower flow rates, while the diffuser system is more comfortable in the higher flow rates.

5 Conclusions

A computational thermal evaluation and comparison between fabric ductwork systems and ceiling diffuser systems is presented in this paper. Transient, fully three dimensional computational (CFD) simulations (involving multiple million unknowns) are performed to compute flow patterns and thermal evolution in rooms containing either conventional or fabric ductwork. High performance computing (HPC) resources were leveraged to efficiently compute the time varying fields to quantitatively compare the two systems. The performance of each system was directly compared on the basis of various metrics of efficiency.

The fabric systems thermally performed better by heating the room faster and more uniformly. The ceiling diffuser system exhibited non-homogeneous heating of the space, resulting in warm and cold areas within the room. The fabric system displayed a breezier space due to the high velocity inlet jets. Our analysis also revealed that the effects of buoyancy can drastically affect the heating of individual spaces. There exists a critical Richardson number that the flow field must overcome to fully heat the room. The fabric system reaches the critical Richardson number earlier than the diffuser system due to the higher flow field velocities. The critical Richardson number influences the mixing within the room and is manifested as mode shifts in the temporal variation of temperature standard deviation within the room. For the flow rates simulated, the inlet flow of the ceiling diffuser system displayed bias towards the outlet, while the fabric system showed no bias. The higher air speeds and the multiple inlets of the fabric system resulted in more energy being absorbed by the room. The fabric system was determined to be 24.5% more efficient than the ceiling diffuser system. The increase in performance of the fabric system shows significant promise towards the use of such fabric ducting systems in the construction of green, energy-efficient buildings.

6 Acknowledgments

This research was supported in part by the National Science Foundation through TeraGrid resources provided by NCSA under grant numbers TG-DMS100021, and TG-CTS110007. AF was funded in part by financial support from DuctSox. The authors thank Prof. Gregory Maxwell for insightful discussions. The authors also thank the anonymous reviewer for several suggestions that improved the paper.

References

- [1] ANSYS FLUENT, 12.1, ANSYS FLUENT Inc., 2009.
- [2] N. BAKER, K. STEEMERS, Energy and Environment in Architecture: A Technical Design Guide, Taylor & Francis Group, London, UK, 2000.
- [3] I. BEAUSOLEIL-MORRISON, The Adaptive coupling of heat and air flow modelling within dynamic whole-building simulation, University of Strathclyde, Glasgow, UK, 2000.
- [4] J. BORGGGAARD, J. A. BURNS, A. SURANA, AND L. ZIETSMAN, Control, estimation and optimization of energy efficient buildings, American Control Conference, 10-12 June 2009, pp. 837–841.
- [5] C.Y.H. CHAO , M.P.WAN, Airflow and air temperature distribution in the occupied region of an underfloor ventilation system, *Building and Environment*, 2004, 39, 749–762.
- [6] Y. A. CENGEL, J. M. CIMBALA, Fluid Mechanics: Fundamentals and Applications, McGraw-Hill, Boston, 2006.
- [7] R. CHOUDHARY, A. MALKAWI, AND P. Y. PAPALAMBROS, Analytic target cascading in simulation-based building design, *Automation in Construction*, 2005, 14, pp. 551–568.
- [8] CUBIT, [online] available:<http://cubit.sandia.gov/> (2010).
- [9] L. A. DAMIANO, D. S. DOUGAN ANSI/ASHRAE Standard 62.1-2004, Encyclopedia of Energy Engineering and Technology, Taylor & Francis Group, Boca Raton, FL, 2004.
- [10] H. FENG, M. OLSEN, Y. LIU, R. FOX, AND J. HILL, Investigation of Turbulent Mixing in a Confined Planar-Jet Reactor, *AIChE Journal*, 2005, 51, 2649–2664.
- [11] W. J. FISK, W. DELP , R. DIAMOND, D. DICKERHOFF, L. RONNEN, M. MODERA, M. NEMATOLLAHI, AND D. WANG, Duct systems in large commercial buildings: physical characterization, air leakage, and heat conduction gains, *Energy and Buildings*, 2000, 32, pp. 109–119.
- [12] G. GROSSMAN, Solar-powered Systems for Cooling, Dehumidification and Air-conditioning, *Solar Energy*, 2002, 72, pp. 53–62.
- [13] Intel 64 Dell Cluster ABE webpage, [online] available: <http://www.ncsa.illinois.edu/UserInfo/Resources/Hardware/Intel64Cluster/> (2010).
- [14] J. KOSNY, T. PETRIE, D. YARBROUGH, P. CHILDS, A. SYED, AND C. BLAIR, Nano-Scale Insulation at Work: Thermal Performance of Thermally Bridged Wood and Steel Structures Insulated with Local Aerogel Insulation, ASHRAE THERM X, Clearwater, FL, December 2007.

- [15] J. KOSNY, D. YARBROUGH, W. MILLER, T. PETRIE, P. CHILDS, A. SYED, AND D. LEUTHOLD, Thermal Performance of PCM-Enhanced Building Envelope Systems, ASHRAE THERM X, Clearwater, FL, December 2007.
- [16] X. LI, B. ZHAO , P. GUAN, AND H. REN, Air Supply Opening Model of Ceiling Diffusers for Numerical Simulation of Indoor Air Distribution under Actual Connected Conditions, *Numerical Heat Transfer*, 2006, 50, 45–61.
- [17] Z. LIN, T. T. CHOW, C. F. TSANG, K.F. FONG, L.S. CHAN, CFD study on effect of the air supply location on the performance of the displacement ventilation system, *Building and Environment*, 2005, 40, 1051–1067.
- [18] Y. LIU, H. FENG, M. OLSEN, R. FOX, AND J. HILL, Turbulent mixing in a confined rectangular wake, *Chemical Engineering Science*, 2006, 61, 6946–6962.
- [19] A. MELIKOV, R. CERMAK, M. MAJER, Personalized ventilation: evaluation of different air terminal devices, *Energy and Buildings*, 2002, 34, 829–836.
- [20] A. NOVOSELAC, J. SREBRIC, A critical review on the performance and design of combined cooled ceiling and displacement ventilation systems, *Energy and Buildings*, 2002, 34, pp. 497–509.
- [21] R. PARSONS, 2001 ASHRAE Handbook: Fundamentals. Atlanta, GA: American Society of Heating, Refrigerating and Air-Conditioning Engineers, 2001.
- [22] S. B. POPE, Turbulent Flows. Cambridge University Press, Boston, MA, 2008.
- [23] J. RUSSO, T. DANG, H. KHALIFA, Computational analysis of reduced-mixing personal ventilation jets, *Building and Environment*., 2009, 44, pp. 1559–1567.
- [24] S. C. SEKHAR, A critical evaluation of variable air volume system in hot and humid climates, *Energy and Buildings*, 1997, 26, pp. 223–232.
- [25] Y. SUN, T. F. SMITH, Air Flow characteristics of a room with square cone diffusers, *Building and Environment*., 2005, 40, pp. 589–600.
- [26] H. SUN, L. ZHAO, AND Y. ZHANG, Evaluating RNG k-[epsilon] models using PIV data for airflow in animal buildings at different ventilation rates, *ASHRAE Transactions*, 2007.
- [27] H. SUN, L. ZHAO, AND Y. ZHANG, Evaluation of RNG k-[epsilon] and LES and Non-Isothermal Models for Indoor Airflow Using PIV Measurement Data, *ASABE Transactions*, 2007, 50, pp. 621–631.
- [28] L. TIAN, Z. LIN, AND Q. WANG, Comparison of gaseous contaminant diffusion under stratum ventilation and under displacement ventilation, *Building and Environment*., 2010, 45, pp. 2035–2046.
- [29] C. P. UNDERWOOD, HVAC Control Systems: Modelling, Analysis and Design, Taylor & Francis Group, London, UK, 1999.
- [30] M. WETTER, Simulation-Based Building Energy Optimization, University of California, Berkeley, CA, 2004.

- [31] X.Q. ZHAI, R.Z. WANG, Y.J. DAI, J.Y. WU, Y.X. XU, AND Q. MA, Solar integrated energy system for a green building, *Energy and Buildings*, 2007, 39, 985–993.
- [32] Z. WU, R. V. N. MELNIK, F. BORUP, Model-based analysis and simulation of airflow control systems of ventilation units in building environments, *Building and Environment*, 2007, 42, 203–217.

Table 1
Nomenclature

Common Nomenclature

c	Speed of sound in the medium
c_p	Specific heat capacity of air
f	Body forces acting on the fluid
g_y	Acceleration due to gravity
Ma	Mach number
t	Time
p	Pressure
T	Temperature of air
T_∞	Temperature of the wall
u	Velocity of air
α	Thermal conductivity of air
β	Thermal expansion coefficient of air
μ	Dynamic viscosity of air
μ_T	Turbulent viscosity of air
σ_t	Turbulent Prandtl number
ρ	Density of air

Table 2
Number of degrees of freedom in each domain for the convergence test

Degrees of Freedom for Convergence Test	
Fabric Ductwork	Ceiling Diffuser
3,424,208	3,590,076
7,216,853	7,129,661
13,600,860	13,744,717

Table 3
Simulation flow rates and inlet Reynolds numbers

N*ASHRAE Min (-)	Volumetric Flow Rate (m^3/s)	Inlet Re Fabric (-)	Inlet Re Diffuser (-)
1	0.00653	3,488	4,069
2	0.01310	6,975	8,138
5	0.03270	17,438	20,344
10	0.06530	34,876	40,688
21	0.14000	69,752	81,377

Table 4
L2 Error norm for convergence

L2 Error norm for convergence				
System	Ceiling Diffuser		Fabric Ductwork	
Discretization (Elements)	512,868	1,018,523	519,921	1,030,979
Mean temperature	8.16e-05	2.66e-05	8.72-05	2.81e-05
Deviation temperature	0.0234	0.0119	0.0801	0.0247
Mean air speed	0.0218	0.0107	0.0511	0.0219
Deviation air speed	0.00338	0.00204	0.0333	0.0114
Power absorbed by room	0.0333	0.0172	0.0280	0.00976

Figure captions

Figure 1: (a) Example of a conventional ductwork system, (b) Example of a fabric ductwork system

Figure 2: Domain of diffuser system (a) near view of the diffuser (b) domain of the fabric system (c) near view of the fabric tube (d)

Figure 3: Iso-contours of temperature of the diffuser system at $t = 50$ seconds for two flow rates. (a) 3D contour at the ASHRAE minimum flow rate, (b) x-plane center slice at the ASHRAE minimum flow rate (c) 3D contour at 21 times the ASHRAE minimum flow rate, and (d) x-plane center slice at 21 times the ASHRAE minimum flow rate.

Figure 4: (a) Mean of the temperature field in the room for the diffuser system under multiple flow rates vs. time, (b) Standard deviation of the temperature field in the room for the diffuser system under multiple flow rates vs. time.

Figure 5: a) Mean of the velocity field in the room for the diffuser system under multiple flow rates vs. time, (b) Standard deviation of the air speed in the room for the diffuser system under multiple flow rates vs. time.

Figure 6: Power absorbed by the room for the (a) diffuser and (b) fabric systems under multiple flow rates vs. time.

Figure 7: Iso-contours of temperature of the fabric system at $t = 50$ seconds for multiple flow rates. (a) 3D contour at the ASHRAE minimum flow rate, (b) x-plane center slice at the ASHRAE minimum flow rate, (c) 3D contour at 5 times the ASHRAE minimum flow rate, (d) x-plane center slice at 5 times the ASHRAE minimum flow rate.

Figure 8: (a) Mean of the temperature field in the room for the fabric system under multiple flow rates vs. time, (b) Standard deviation of the temperature field in the room for the fabric system under multiple flow rates vs. time

Figure 9: (a) Mean of the velocity field in the room for the fabric system under multiple flow rates vs. time, (b) Standard deviation of the air speed in the room for the fabric system under multiple flow rates vs. time

Figure 10: The Richardson Number for the fabric and diffuser system for the simulated flow rates at $t = 50$ seconds

Figure 11: Iso-contours of temperature of the (a) diffuser system at $t = 10$ seconds, (b) fabric system at $t = 10$ seconds, (c) diffuser system at $t = 30$ seconds, (d) fabric system at $t = 30$ seconds, (e) diffuser system at $t = 50$ seconds, (f) fabric system at $t = 50$ seconds.

Figure 12: Temperature contour slice of the center x-plane (a) diffuser system at $t = 10$ seconds, (b) fabric system at $t = 10$ seconds, (c) diffuser system at $t = 30$ seconds, (d) fabric system at $t = 30$ seconds, (e) diffuser system at $t = 50$ seconds, (f) fabric system at $t = 50$ seconds.

Figure 13: (a) Mean of the temperature field in the room for both the diffuser and fabric system vs. time, (b) Standard deviation of the temperature field in the room for both the diffuser and fabric system vs. time.

Figure 14: (a) Mean of the velocity field in the room for both the diffuser and fabric system vs. time, (b) Standard deviation of the velocity field in the room for both the diffuser and fabric system vs. time.

Figure 15: Power absorbed by the room for the diffuser and fabric systems vs. time.

Figure 16: Air Distribution Performance Index for the Fabric and Diffuser ductwork systems for multiple flow rates.



(a)



(b)

Fig. 1. (a) Example of a conventional ductwork system, (b) Example of a fabric ductwork system

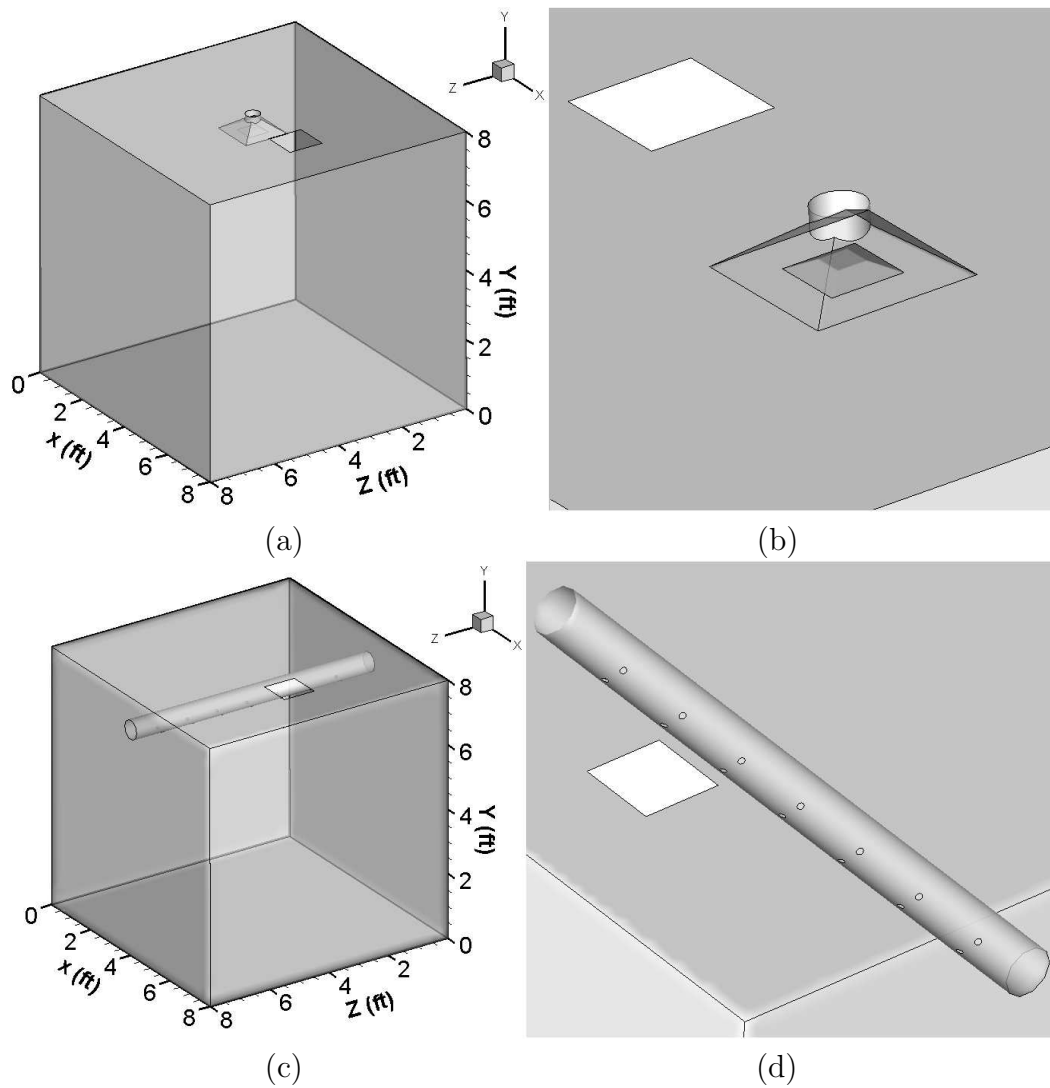


Fig. 2. Domain of diffuser system (a) near view of the diffuser (b) domain of the fabric system (c) near view of the fabric tube (d)

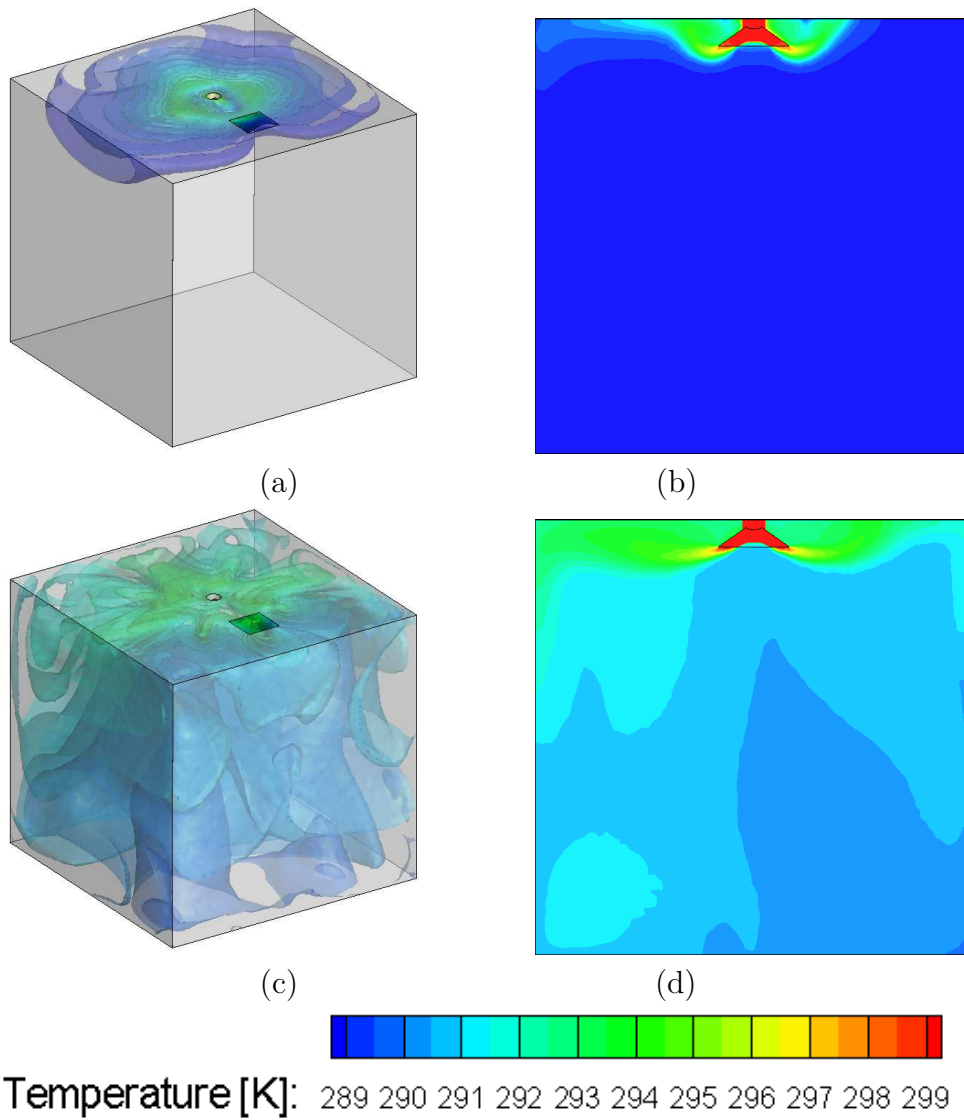


Fig. 3. Iso-contours of temperature of the diffuser system at $t = 50$ seconds for two flow rates. (a) 3D contour at the ASHRAE minimum flow rate, (b) x-plane center slice at the ASHRAE minimum flow rate (c) 3D contour at 21 times the ASHRAE minimum flow rate, and (d) x-plane center slice at 21 times the ASHRAE minimum flow rate.

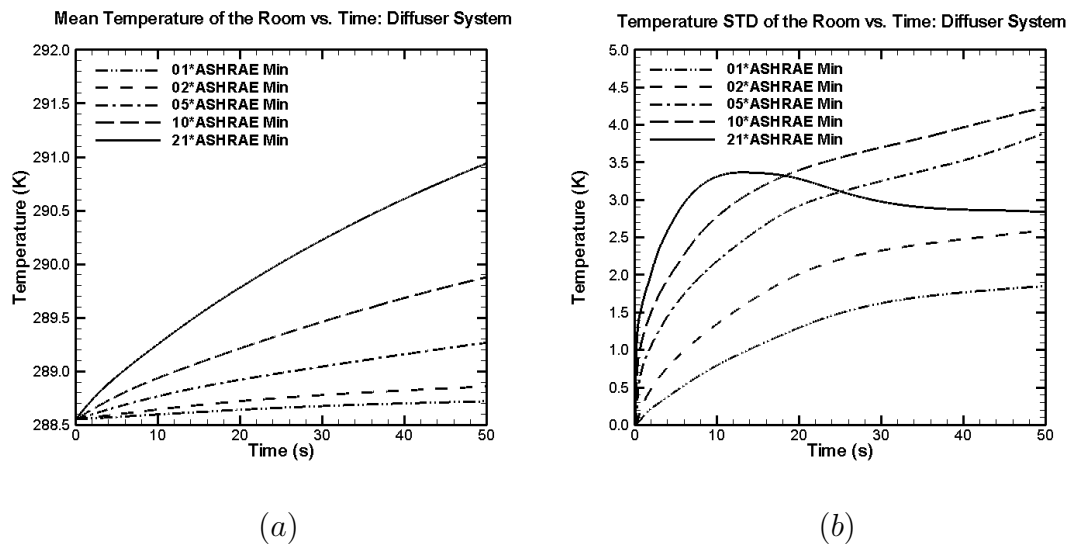
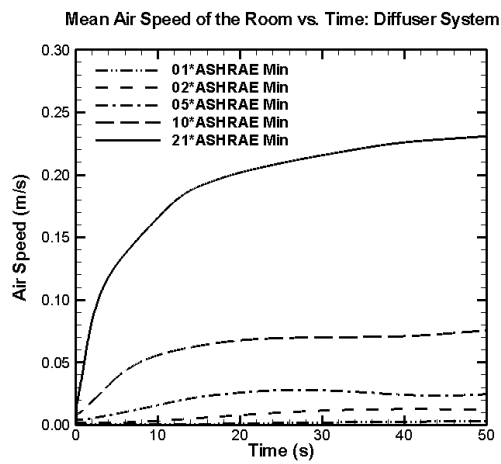
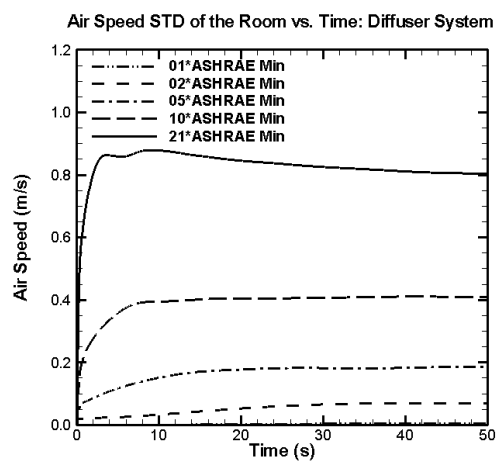


Fig. 4. (a) Mean of the temperature field in the room for the diffuser system under multiple flow rates vs. time, (b) Standard deviation of the temperature field in the room for the diffuser system under multiple flow rates vs. time.

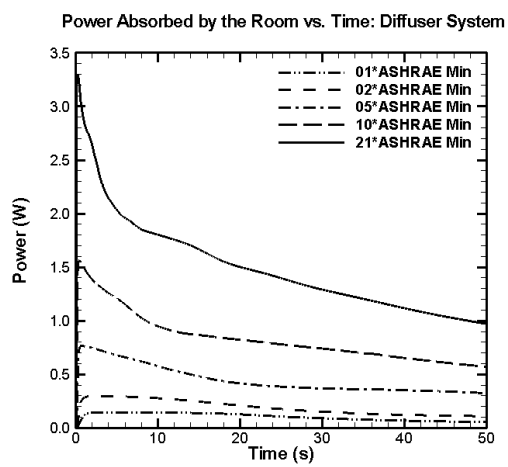


(a)

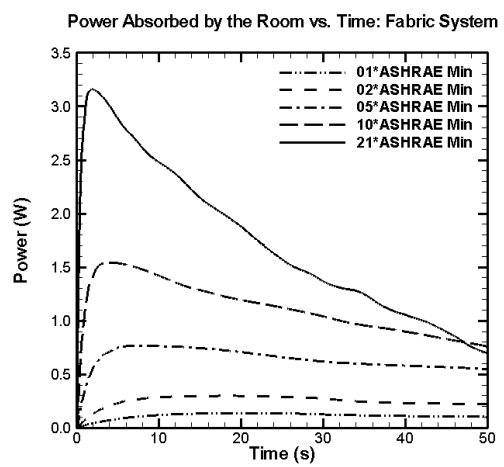


(b)

Fig. 5. (a) Mean of the velocity field in the room for the diffuser system under multiple flow rates vs. time, (b) Standard deviation of the air speed in the room for the diffuser system under multiple flow rates vs. time.



(a)



(b)

Fig. 6. Power absorbed by the room for the (a) diffuser and (b) fabric systems under multiple flow rates vs. time.

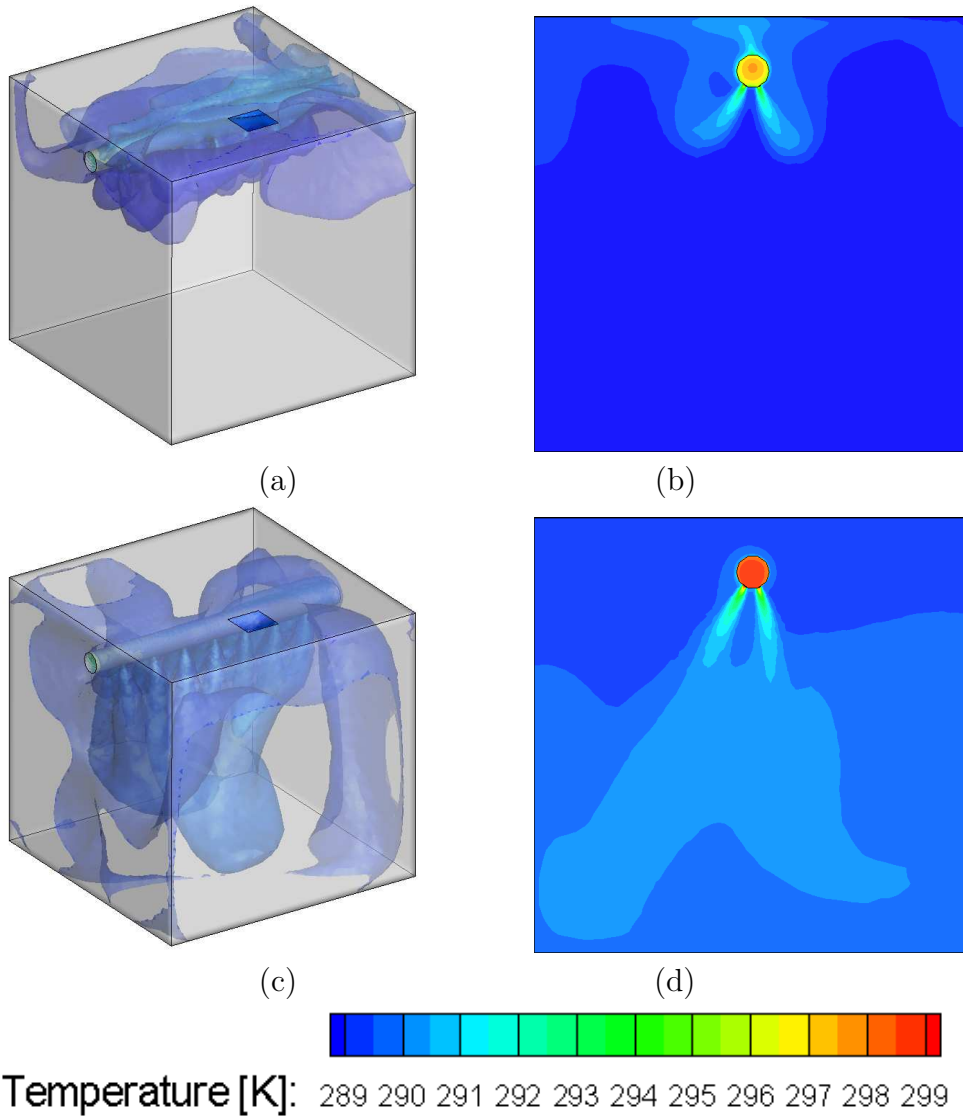
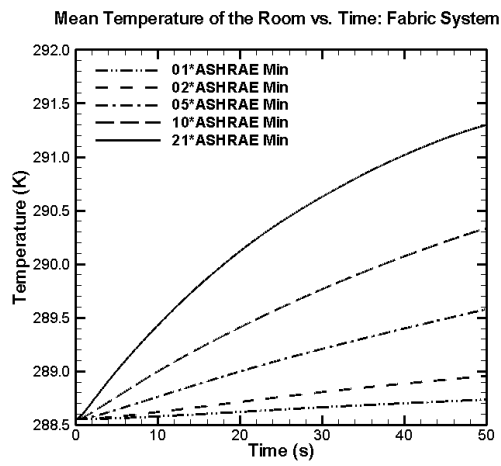
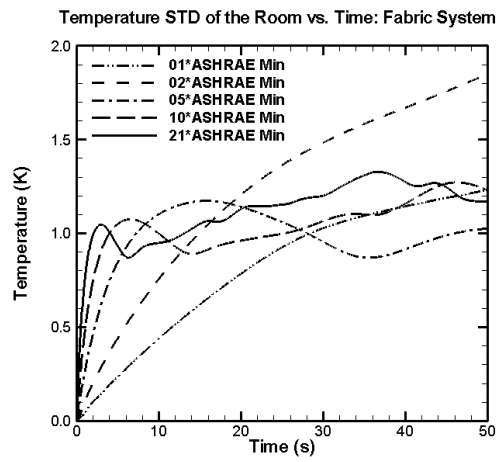


Fig. 7. Iso-contours of temperature of the fabric system at $t = 50$ seconds for multiple flow rates. (a) 3D contour at the ASHRAE minimum flow rate, (b) x-plane center slice at the ASHRAE minimum flow rate, (c) 3D contour at 5 times the ASHRAE minimum flow rate, (d) x-plane center slice at 5 times the ASHRAE minimum flow rate.

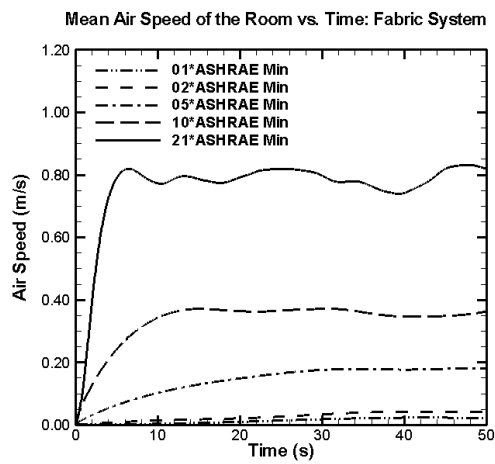


(a)

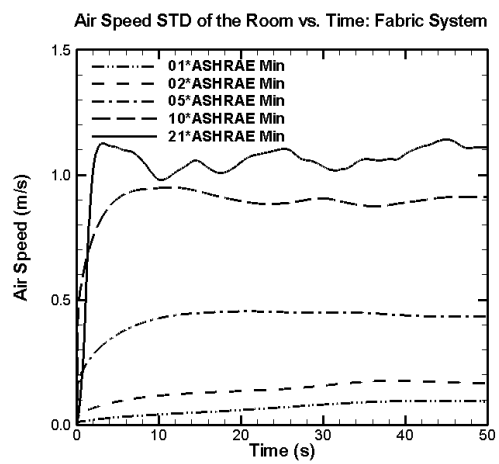


(b)

Fig. 8. (a) Mean of the temperature field in the room for the fabric system under multiple flow rates vs. time, (b) Standard deviation of the temperature field in the room for the fabric system under multiple flow rates vs. time



(a)



(b)

Fig. 9. (a) Mean of the velocity field in the room for the fabric system under multiple flow rates vs. time, (b) Standard deviation of the air speed in the room for the fabric system under multiple flow rates vs. time

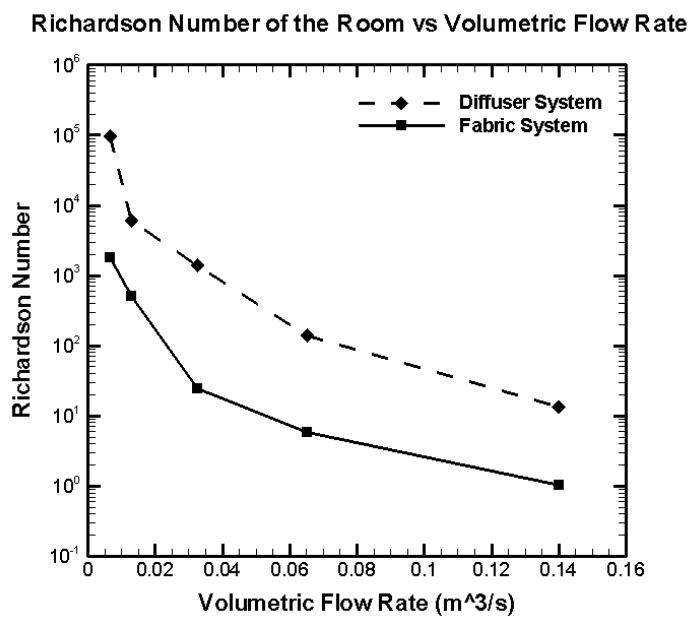


Fig. 10. The Richardson Number for the fabric and diffuser system for the simulated flow rates at $t = 50$ seconds

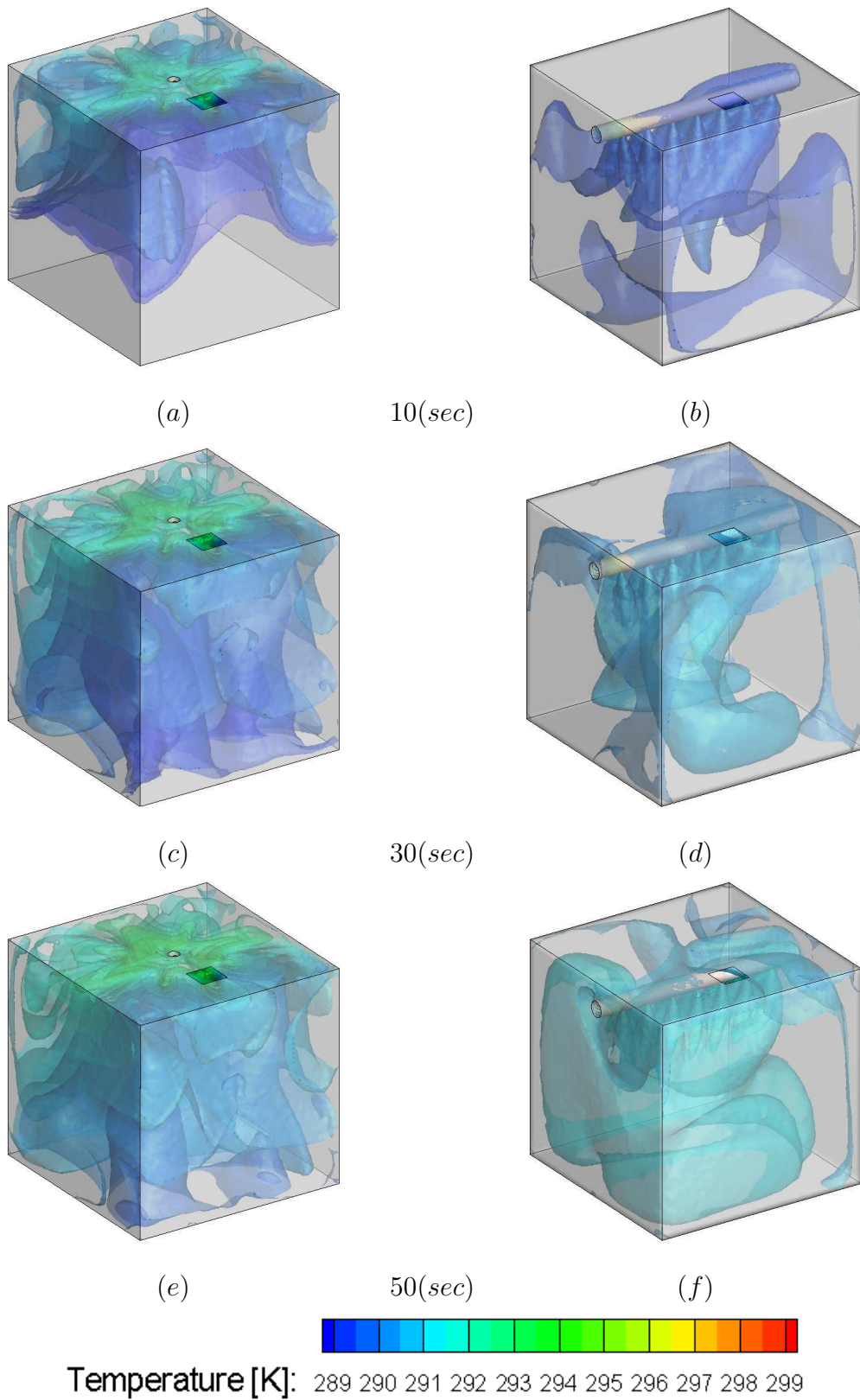


Fig. 11. Iso-contours of temperature of the (a) diffuser system at $t = 10$ seconds, (b) fabric system at $t = 10$ seconds, (c) diffuser system at $t = 30$ seconds, (d) fabric system at $t = 30$ seconds, (e) diffuser system at $t = 50$ seconds, (f) fabric system at $t = 50$ seconds.

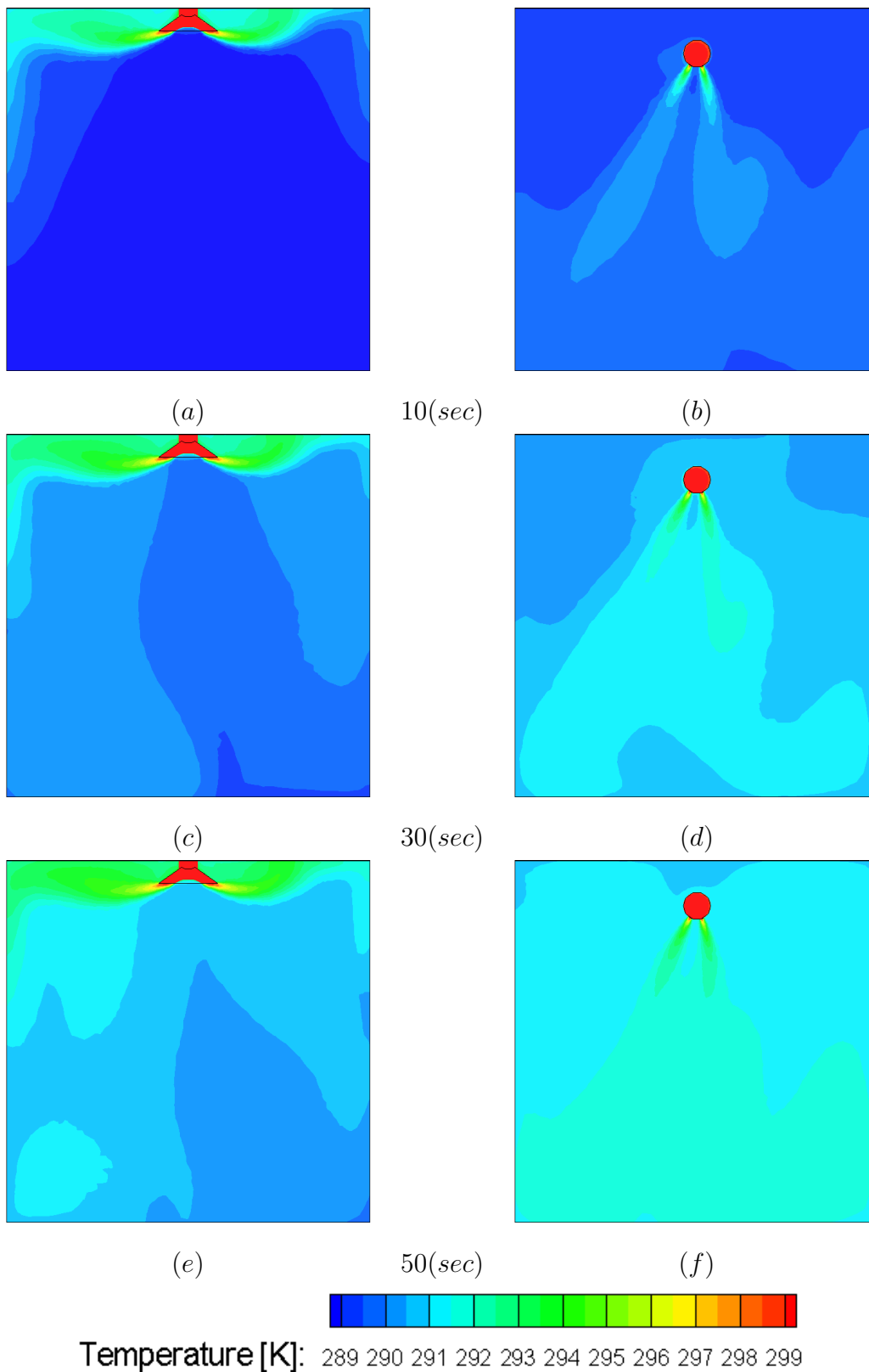


Fig. 12. Temperature contour slice of the center x-plane (a) diffuser system at $t = 10$ seconds, (b) fabric system at $t = 10$ seconds, (c) diffuser system at $t = 30$ seconds, (d) fabric system at $t = 30$ seconds, (e) diffuser system at $t = 50$ seconds, (f) fabric system at $t = 50$ seconds.

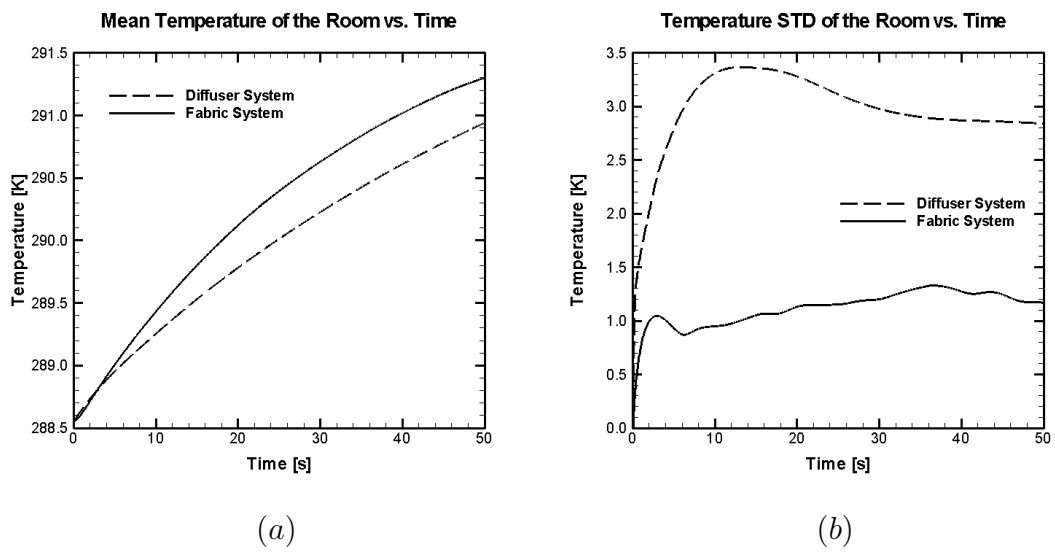
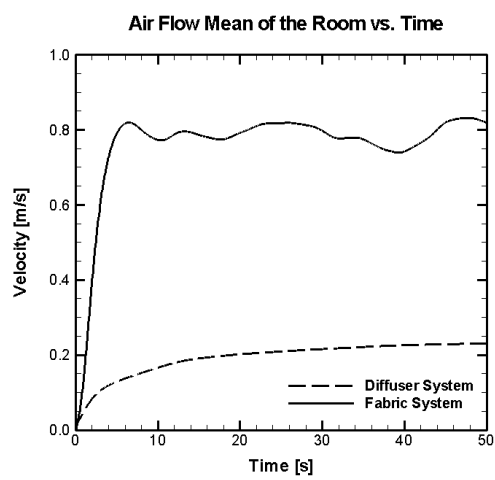
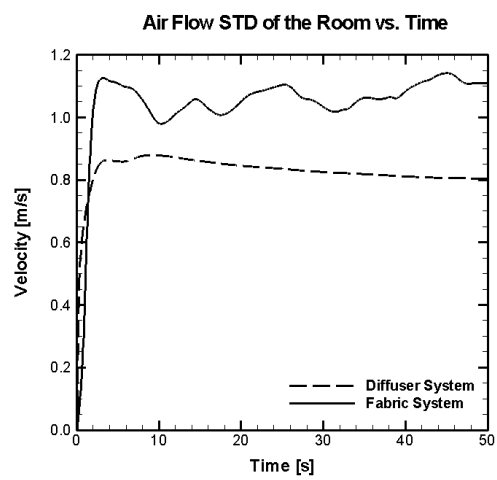


Fig. 13. (a) Mean of the temperature field in the room for both the diffuser and fabric system vs. time, (b) Standard deviation of the temperature field in the room for both the diffuser and fabric system vs. time.



(a)



(b)

Fig. 14. (a) Mean of the velocity field in the room for both the diffuser and fabric system vs. time, (b) Standard deviation of the velocity field in the room for both the diffuser and fabric system vs. time.

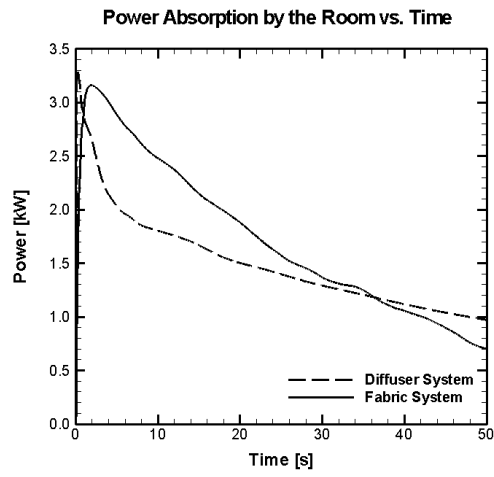


Fig. 15. Power absorbed by the room for the diffuser and fabric systems vs. time.

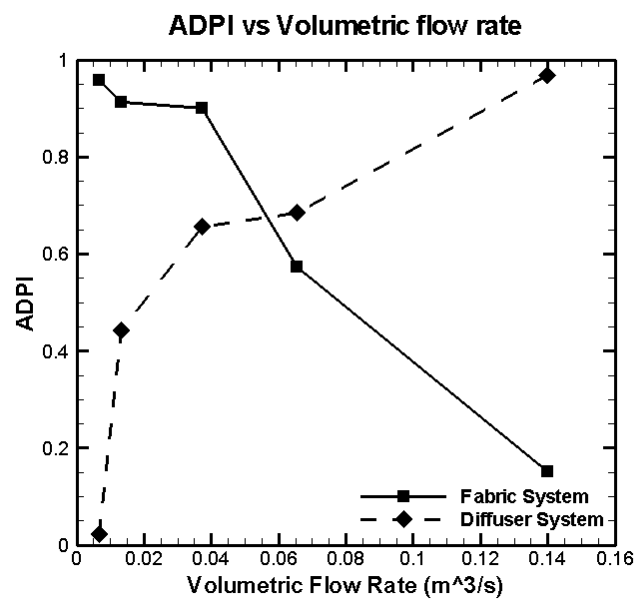


Fig. 16. Air Distribution Performance Index for the Fabric and Diffuser ductwork systems for multiple flow rates.